Vibrational modes and overlap matrix of $LiNb_{1-x}Ta_xO_3$ mixed crystals

A. Bartasyte,[1,2#] S. Margueron,[2] A.M. Glazer,[1] E. Simon,[3] I. Gregora,[4] S. Huband,[5] and P.A. Thomas[5]

[1]Department of Physics, Oxford University, Parks Road, Oxford OX1 3PU, UK

[2]Institute FEMTO-ST, CNRS (UMR 6198)-University of Bourgogne Franche-Comté, 26 rue de l'Epitaphe, 25030 Besançon, France

[3] Department of Physics, BCM College, Kottayam, Kerala, India

[4] Institute of Physics, ASCR, Prague 8, Czech Republic

[5]Department of Physics, University of Warwick, Coventry, UK

Abstract

The wavenumbers and efficiencies of the first-order lattice vibrational modes of the isomorphous solid solutions of $LiNbO_3$-$LiTaO_3$ have been studied by Raman and infrared spectroscopies. The substitution of niobium by tantalum induces a continuous shift of wavenumbers and intensities of phonon modes indicating a one-phonon behaviour. In general, the wavenumbers of vibrations at low frequencies (< 325 cm^{-1}) soften with the increased atomic mass. The frequencies of most of the high-frequency modes increase with the Ta/Nb ratio owing to enhanced force constants. A qualitative relation between the shift of transverse and longitudinal modes in the solid solutions has been found on the basis of an overlap matrix. The exceptional softening of several high-frequency modes with the replacement of Nb by Ta originates from the strong interaction of these modes with modes at low frequencies according to the overlap matrix. The intensities of the Raman modes are strongly modulated by the electronic properties with Ta/Nb substitution and this emphasises their role in the physical properties of $LiNbO_3$ and $LiTaO_3$.

ausrine.bartasyte@femto-st.fr

Introduction

Lithium niobate ($LiNbO_3$, LN) and lithium tantalate ($LiTaO_3$, LT) are two of the most important materials used in the fields of optics, electro-optics and acoustics. At room temperature LN and LT are isomorphous and ferroelectric, crystallizing in the space group R3c [1,2]. The ferroelectric LN and LT crystal structure can be described in terms of polar displacements of the cations along the [0001] direction, with corner-linked oxygen octahedra tilted according to the system $a^-a^-a^-$[3]. Despite the structural similarity of LT and LN, these materials show different physical properties [4,5,6]. In particular, LT (with congruent composition) has a low Curie temperature (603 °C), a high melting point (1650°C), a wide bandgap (4.8 eV) and a positive optical birefringence, whereas congruent LN has a high Curie temperature (1133 °C) close to the melting point (1253°C), a bandgap of 3.8 eV, and a negative optical birefringence. LN presents much stronger anisotropy of the static dielectric constant than LT. Therefore, $LiNb_{1-x}Ta_xO_3$ (LNT_x) materials are of special interest because their properties can be tuned between those of LN and LT [7,8]. Thus this strong difference makes these materials very attractive for applications in the THz range.

At room temperature, in space group R3c, there are 10 ions per unit cell, and so LN, LT and LNT have 30 degrees of freedom. At the Γ point the irreducible representations are given by $5A_1 + 5A_2 + 10E$. The A_1 modes are infra-red (IR) active while the remaining modes are both Raman and IR active. Of these $4A_1+5A_2+9E$ modes correspond to optical phonons. A_1 modes are polarized along *Z*-axis and the doubly-degenerate E modes are polarized in the *X*-*Y* plane. All the phonons of LN-LT are polar; thus they are split into transverse (TO) and longitudinal (LO) modes. The TO-LO splitting depends on the magnitude of the long-range electrostatic forces. It is known that the difference in Raman-scattered intensities between TO and LO modes in piezoelectric crystals may be attributed to the electro-optic effect. Moreover, in a uniaxial crystal, a mode associated with a certain component of the Raman tensor may vary in frequency depending on the direction of its propagation relative to the optic axis. At arbitrary angles θ with the c-axis ($\theta \neq 0°$ and 90°), the direction-dependent modes are not pure (quasimodes or oblique modes). If the dominant forces in crystal dynamics are short-range and anisotropic, these quasimodes do not have definite LO or TO polarizations. In the electrostatic (long-range) approximation, the modes do not have single A_1- or E-symmetry.

The dynamical properties of the end members, LN and LT, have been intensively studied. There are numerous reports concerning optical phonons in LT and LN, studied by Raman [9,10,11,12,13] and infrared spectroscopies [14,15], neutron inelastic scattering [16] and theoretically [17,18,19]. Recently, a complete assignment of E-symmetry modes in LN and LT has been achieved experimentally by comparing Raman and IR data [9] and theoretically [17,20]. The directional dispersion of the extraordinary phonons of LN and LT taking into account this new assignment is still not reported. Little is known about the absolute Raman efficiency of these crystals, as well.

Generally speaking, the dynamical properties of different types of solid solutions have been extensively studied in literature. Physical models describing the optical properties of mixed crystals have been summarized by Elliott et al. [21]. Nevertheless, few reports have been found on LNT solid-solution zone-centre phonons [22,23]. Ge et al. [22] studied only $LNT_{0.9}$, and claimed that the Raman mode assignment is similar to that of LT. Sanna et al. [23,24] predicted theoretically the linear shift of A_1(TO) and E(TO) modes as a function of Nb/Ta ratio in LNT_x solid solutions by using density functional theory (DFT). DFT have not been applied to calculate the shifts of A_1(LO) and E(LO) modes with the composition change. The zone-centre phonons as a function of Ta/Nb ratio have been studied experimentally, as well [24]. However, the DFT was not sufficient to explain the frequency change of several A_1(TO) and E(TO) modes with Ta/Nb composition. The relationship between the lattice vibration modes of LN and LT remains insufficiently investigated to date. The optical phonon frequencies, damping parameters, and intensities are of special interest in studies of phase transitions, symmetry, effect of pressure, stress [25], composition [26] and heterogeneities in thin films [27], integrated structures [28], and in nano and bulk materials. It is essential to know the frequencies for calculations of dielectric constant [29], oblique modes [30], and electro-optic coefficients [31].

In this paper, all 27 optical phonons at the Γ point of LNT_x single crystals are identified by using two complimentary techniques: unpolarized IR and polarized Raman spectroscopies. The effect of Nb replacement by Ta on the wavenumbers, coefficients of Raman tensor/Raman efficiency, oblique mode dispersions and overlap matrix of the zone-centre phonons over the whole composition range $0 \leq x \leq 1$ is described below.

Experimental details

Li_2CO_3 (99.9 %), Nb_2O_5 (99.9 %) and Ta_2O_5 (99.9 %), supplied by Johnson Matthey (UK), were used as starting materials for single-crystal growth and synthesis of powders. The stoichiometric LNT_x powders with different Ta/Nb compositions were sintered for 130 hours at 1160 °C in sealed platinum crucibles. The LN and LT congruent compositions are non-stoichiometric (48.6 and 49 % of Li_2O, respectively), while the congruent compositions of LNT solid solutions are unknown. Thus, congruent LNT_x crystals were grown from melts with intermediate Li_2O compositions (48.6 + 0.4x). Congruent $LNT_{0.18}$, $LNT_{0.31}$ and $LNT_{0.43}$ single crystals were grown by the Czochralski method. Nearly stoichiometric $LNT_{0.67}$ single crystals were synthesized by using top-seeded solution growth. More details about synthesis of powders and single crystals are given in by Bartasyte *et al*. [32].

The as-grown LNT_x crystals with homogeneous Ta and Nb ratios (within EDAX analysis limits) were oriented using back-reflection X-ray Laue photographs. Optically polished plates were then prepared with the three-fold axis lying in the plane of the plate or perpendicular to it. No other constraints were placed on the orientations of the samples. For the two end-members of the solid solution series, commercially grown and oriented LN and LT crystals with congruent Li concentrations were used (supplied by MTI Corporation).

Raman spectra were collected using Jobin-Yvon/Horiba LabRam and Renishaw Raman RM-1000 spectrometers. Experiments were conducted in the micro-Raman mode in backscattering geometry. The 514.5 nm line of an Ar^+ ion laser was focused to a spot size of about 1 μm using two Olympus objectives: ×100 (N.A. = 0.9) and ×50 long working distance (LWD, N.A. = 0.5). The spectra were calibrated using Si spectra at room temperature (RT). To extract the parameters of the Raman peaks, the spectra were fitted with a response function containing a constant baseline and a sum of independent harmonic oscillator contributions multiplied by the Bose-Einstein temperature factor.

In order to estimate the absolute values of the coefficients of the Raman efficiency, the polarized Raman spectra of LN and LT single crystals were measured under crossed and parallel polarization configurations (VH and VV, respectively) and under identical experimental conditions (laser power, acquisition time, alignment of the system, objective …). The areas under the mode profiles, representing the Raman efficiency, $I_{measured}$, were corrected for the effect of the instrumental function by

$$I_{corrected} = I_{measured} \frac{I_{unpolarized\ spectrum\ of\ lamp}}{I_{VV\ or\ VH\ spectrum\ of\ lamp}}, \quad (1)$$

$I_{\text{unpolarized spectrum of lamp}}$ and $I_{\text{VV or VH spectrum of lamp}}$ are the intensities of a calibrated lamp measured with unpolarized light and under VV or VH polarization configurations, respectively. The absolute intensity of the spectra was calibrated with respect to a benzene spectrum measured under identical experimental conditions. The polarization configurations and fitting parameters used for the determination of the *a, a′, b, c, c′, d* coefficients (primes indicate that the coefficient contains also a contribution from the electro-optic interaction) are summarized in Table I.

IR reflectivity measurements were performed using an FTIR spectrometer Bruker IFS 113v. Room-temperature spectra were taken in the range 30–3000 cm^{-1} with a resolution of 2 cm^{-1}. The unpolarized near-normal reflectivity spectra $R(\omega)$ were taken from the polished surface of several mm thick Z-cut crystals so that the measured spectra could be analyzed with a simple Fresnel relation

$$R(\omega) = \left|\frac{\sqrt{\varepsilon(\omega)}-1}{\sqrt{\varepsilon(\omega)}+1}\right|^2 \quad (2)$$

involving solely the ordinary complex permittivity spectrum $[\varepsilon(\omega) = \varepsilon'(\omega) - i\varepsilon''(\omega)]$ defined by E-symmetry modes only. IR reflectivity spectra were fitted assuming the standard factorized form of the oscillator model for the complex permittivity

$$\varepsilon(\omega) = \varepsilon_\infty \prod_{j=1}^{n} \frac{\omega_{LOj}^2 - \omega^2 + i\omega\gamma_{LOj}}{\omega_{TOj}^2 - \omega^2 + i\omega\gamma_{TOj}} \quad (3)$$

Here ω_{TOj} and ω_{LOj} mark the transverse and longitudinal frequencies of the j^{th} mode, respectively, and γ_{TOj} and γ_{TOj} denote their corresponding damping.

If the TO and LO frequencies of all pure polar modes (as well as the corresponding permitivities) are known, the eigenvector and eigenfrequency of any (long-wavelength) polar mode for arbitrary propagation direction and the coefficients (overlap matrix) describing the contribution of pure modes to any mode in question can be calculated in terms of the eigenvectors of pure TO modes by solving a set of coupled linear equations [33]. This is a consequence of the fact that all polar modes are coupled by macroscopic electric field, which in turn depends on longitudinal polarization screened by high-frequency dielectric response appropriate for the field along the propagation direction. In this way the "overlap matrices", the columns of which represent the normalized eigenvectors of all LO modes in the basis of all TO modes, were calculated by using method described by Shapiro and Axe [33] for propagation along the c-axis (A_1 modes) and perpendicular to it (E modes) in $LiNbO_3$ and $LiTaO_3$ (see Table V and VI) and

also for the mixed $LiNb_{0.57}Ta_{0.43}O_3$ ($LNT_{0.43}$). Ordinary and extraordinary refractive indexes (n_o and n_e, respectively), used in the calculations, were: n_o(LN) = 2.288, n_e(LN) = 2.203, n_o(LT) = 2.179, n_e(LT) = 2.182, n_o($LNT_{0.43}$) = 2.241 and n_e($LNT_{0.43}$) = 2.194.

Results

In LNT_x solid solutions, the dynamical properties are influenced not only by the Ta/Nb ratio but also by Li nonstoichiometry. The quality and stoichiometry may vary from crystal to crystal as congruent compositions were not known for the mixed crystals. Therefore, first, unpolarized Raman spectra of stoichiometric LNT_x powders with different x, synthesized under identical conditions were studied (Fig.1). E(TO), E(LO), A_1(LO), A_1(TO) and distributions of the oblique modes were observed in the unpolarised spectra of powders. The Raman spectra (wavenumbers and intensity of modes) changed continuously all the way across the solid solution range. No abrupt changes were observed over the whole solid solution range, confirming that the mixed crystals were isostructural with the end members. The identification of some modes in the unpolarized spectra of powders was confusing because of numerous modes with close wavenumbers, especially in the 200 – 300 cm^{-1} range. The asymmetric profiles of Raman modes, related to the distributions of oblique modes, made the fitting procedure complicated. In particular, the E(1TO) and A_1(1TO) mode profiles in the Raman spectra of the powders were highly asymmetric, as the directional dispersion of these modes is especially pronounced.

More accurate assignment of the modes was achieved from the polarized Raman spectra of LNT_x single crystals. The Raman spectra of LNT_x single crystals, with the c-axis in the plane or perpendicular to the plane of surface, were measured in $X(ZZ)\bar{X}$, $Z(XX)\bar{Z}$, $Z(XY)\bar{Z}$ and $X(ZY)\bar{X}$ polarization configurations (Porto's notation) and are presented in Fig. 2, Fig. 3 and Fig. 4, respectively. The modes of the LNT_x single crystals strictly obeyed the Raman selection rules in these polarization configurations. This confirms that the basic symmetry of LN and LT was retained in the LNT_x crystals, as well. The polarized spectra consisted dominantly of first-order modes.

The wavenumbers of A_1(TO), A_1(LO) and E(TO) modes were determined by fitting $X(ZZ)\bar{X}$, $Z(XX)\bar{Z}$ and $X(ZY)\bar{X}$ (or $Z(XY)\bar{Z}$) Raman spectra (given in Fig. 2, Fig. 3 and Fig. 4) and are presented in Table II and Table III, respectively. E(TO) mode wavenumbers were also estimated from unpolarized near –normal reflectivity spectra (Fig. 5) and are compared with Raman data in Table III. The wavenumbers of four A_1(LO), four A_1(LO) and seven E(TO) modes

were determined from Raman spectra of LNTx single crystals with all compositions studied. Eight E(TO) modes were observed in the IR spectra of the mixed crystals. The E(5TO) mode of LNT_x had too low a Raman efficiency and E(6TO) had too low an oscillator strength to be identified in the Raman and IR spectra collected at room temperature. Similar observations were reported for the E(5TO) and E(6TO) modes of the end members [9]. The E(9TO) mode at 657 cm^{-1} in $Z(XY)\bar{Z}$ Raman spectra has a considerably higher relative intensity with respect to the intensity of E(1TO) in the same spectra than that seen in $X(ZY)\bar{X}$ spectra (Fig. 4). The intensity of the E(9TO) mode decreases drastically when Ta is replaced by Nb. This mode has very low intensity in $LNT_{0.30}$, $LNT_{0.18}$ and LN crystals. Its wavenumber in Nb-rich crystals can only be estimated approximately from $Z(XY)\bar{Z}$ spectra. Nevertheless, it can be seen that the mode corresponding to that at 657 cm^{-1} of LT is a mode at around 660 cm^{-1} in LN (Fig. 1 and 4) [9]. The E(9TO) mode was observed at 667 – 663 cm^{-1} in IR spectra in LN, LNT_x and LT crystals, as well.

In backscattering geometry E(LO) modes can be observed together with A_1(TO) modes in $Y(XX)\bar{Y}$ Raman spectra. In LNT_x crystals with the *c*-axis in the plane, the *X*- and *Y*-axes were not in any particular orientation (not perpendicular to the surface plane). Thus, it was not possible to measure proper $Y(XX)\bar{Y}$ and $X(YY)\bar{X}$ polarization configurations. The spectra, measured in these configurations, contained A_1(TO), E(TO) and E(LO) modes. The ratios of E(TO) and E(LO) mode intensities varied from sample to sample because of the different *X*/*Y* axis orientations. This made it difficult to identify E(LO) modes of the mixed crystals from the Raman spectra. The wavenumbers of eight E(LO) modes of the mixed crystals were determined from IR spectra (Fig. 5) and are given in Table IV. The E(5LO) mode was not observed in IR spectra of LNT_x crystals because of its low oscillator strength.

The change of mode wavenumbers with Ta/Nb ratio (Fig. 6) corresponds well with those observed in LNT_x powders and is in a good agreement with literature data [24]. The concentration dependence of the E and A phonon frequencies represents a gradual transformation of frequencies of LN into the frequencies of LT. Basically, the sequence of Raman modes in LN and LT are the same. The only exceptions are crossings between A_1(1TO) and E(2LO)/E(2TO) and between E(4LO) and A_1(2LO)/A_1(3TO). The frequencies of the A_1- symmetry phonons decrease as Nb is replaced by Ta with the exception of increased frequency of A_1(3TO) and A_1(2LO) modes. The frequencies of the E-phonons with wavenumbers lower than 325 cm^{-1} or

higher than 650 cm^{-1} diminish as the Ta/Nb ratio increases. At wavenumbers in the range from 325 to 650 cm^{-1}, the wavenumbers of E modes increase with increasing Ta concentration.

No new frequency bands resulting from overlap of local modes appeared. This indicates that the perturbation resulting from substitution of Nb by Ta (the mass and/or force constant changes are not large) is not sufficiently strong to result in splitting of the vibrational states of the local modes. Behaviour of this type is called one-mode behaviour [20]. Extra impurity modes, associated with clustering effects at finite concentrations, were not observed. The frequencies of E(LO) modes vary smoothly all the way across the concentration range. The IR data confirm one-mode behaviour of LN-LT solid solutions: no local modes occurred in the mixed crystals in the frequency ranges where none occur in the pure crystal.

The eigenvectors of the overlap matrices for the A_1(LO) and A_1(TO) modes and between eigenvectors of the E(TO) and E(LO) modes of LN and LT were calculated from the attribution of all modes and are given in Table V and Table VI, respectively. The overlap eigenvectors are similar in LN and LT. The most important overlap eigenvectors occur between the same groups of modes in LN and LT. The difference between the overlap coefficients of the same modes of LN and LT (Δo) is smaller than 0.13. Exceptions are the stronger overlap between eigenvectors (Δo = 0.2 - 0.3) of A_1(1LO) and A_1(1TO)), A_1(3LO) - A_1(2TO), E(8LO)-E(8TO) and E(9LO) – E(9TO) modes and weaker overlap (Δo = -0.16 - -0.30) of A_1(2LO) – A_1(1TO), A_1(3LO) – A_1(3TO) and E(7LO)-E(7TO) in LN than in LT. As predicted by theory,[17] through the long-range Coulomb interaction, the overlap of eigenvectors of A_1 modes is weak, while mixing is more important for E-symmetry modes in LT and LN. Very weak mixing was observed for A_1(2TO), A_1(3TO), E(2TO), E(6TO) and E(9TO) modes in both materials. These modes are associated with A_1(1LO), A_1(2LO), E(2LO), E(5LO) and E(8LO), respectively. In LN, the experimental overlap coefficients of the eigenvectors agree well with those calculated theoretically [17] (Δo < 0.2). However, the stronger overlap between A_1(1TO) and A_1(2LO), A_1(3TO) – A_1(3LO), E(1LO) – E(2TO) and E(2LO) – E(1TO) modes was expected theoretically.

The behaviour of LNT_x phonon modes can be understood by analysing the overlap matrices between the eigenvectors of the A_1(LO) and A_1(TO) modes and between the eigenvectors of the E(TO) and E(LO) modes of LN and LT (Table V and VI). Overlap between the eigenvectors of transverse and longitudinal E and A_1 modes is summarized in Fig. 7. The eigenvector of the A_1(3LO) mode is mainly defined by that of the A_1(1TO) mode. Thus, like the low-frequency

modes, this mode softens when Nb is replaced by Ta. The vibrations related to the A_1(4TO) mode are mainly designated by the eigenvectors of the A_1(3LO) and A_1(4LO) modes, which have an important overlap with A_1(1TO), as well. Therefore, A_1(4TO) and A_1(4LO) shifts to lower wavenumbers with increase of Ta concentration. In the same way, a shift to lower wavenumbers of the E(4TO) mode is expected. Nevertheless, this qualitative analysis is not sufficient to explain the softening of the E(9LO) mode, which involves a strong overlap with the E(8TO) mode. Therefore, the shift of the j^{th} TO (LO) mode was calculated using the weight coefficient of the LO (TO) modes using the overlap matrix and the relative shift in frequency in the solid solution. The weighted shift, g_j, taking into account the interdependence of modes, was then defined as follows:

$$g_j = \sum_i o_{ij} \frac{\Delta \nu_i}{\overline{\nu_i}} \qquad (4)$$

Where o_{ij} – overlap integral between eigenvectors of i^{th} and j^{th} modes, $\Delta \nu_i$ – the difference in wavenumbers of mode i of LN and LT, and $\overline{\nu_i}$ - the mean wavenumber of i^{th} mode of LN-LT used as a normalization factor. The calculated weight shifts of E and A_1 modes are given in Fig. 7. The sign of g_j indicates a softening or hardening of the mode. The change of frequencies predicted by the weighted shift function corresponds well with that observed experimentally (Fig. 7). In conclusion, g_j is a good criterion to predict the softening and hardening of modes for mixed systems. The E(5LO) mode was not observed at room temperature. Nevertheless, the shift of this mode to higher wavenumbers, when Ta replaces Nb, might be predicted qualitatively.

The directional dispersion of extraordinary phonons of LN, $LNT_{0.43}$ and LT was calculated from experimentally estimated A- and E-phonon frequencies and the refractive indexes of these materials. The complete directional dispersion of all polar modes in LN, LT and $LNT_{0.43}$ is shown in Fig. 8 as a function of the angle of propagation with respect to the *c*-axis. The green lines show the dispersion of the oblique mode frequencies. In general, these modes are of mixed character: neither pure TO or LO, nor pure A_1 or E. The dashed (red) horizontal lines show pure "ordinary" E(TO) modes, exhibiting no directional dispersion. LN, LT and their solid solutions present 13 branches of oblique phonons. The directional dispersions of 1^{st}, 4^{th}, 5^{th}, and 8-13^{th} branches of the end-members and their solid solutions are of the same type and their angular dependence changes smoothly when Nb is replaced by Ta across all the compositional range of the solid solutions. Nevertheless, a significant decrease was observed in the angular dependence of the 11^{th} and 10^{th} branches and in the increased variation of frequency of the 3^{rd}

and 9th branches when the Nb is replaced by Ta. Crystals with Ta/(Ta+Nb) < 50 mol% present seven dispersion branches with E-symmetry, two branches of A-symmetry, two oblique modes with LO polarization and two with TO polarization (Fig. 8). The dominant A- and E-symmetry of the oblique phonons shows that short-range anisotropic forces dominate over electrostatic forces in the dynamics of LN and Nb-rich mixed crystals. At about Ta/(Ta+Nb) = 50 mol%, the frequency of the A_1(2LO) and A_1(3TO) modes crosses the frequency of the E(4LO) mode (Fig. 8). Thus, in the case of Ta-rich solid solutions, two oblique modes with A- and E-symmetry ((6) and (7) branches) lose their A and E-symmetry and transform to LO and TO oblique modes, respectively (Fig. 8). This indicates that the replacement of Nb by Ta increases the long-range electrostatic forces. The 2nd and 3rd branches of the end-member LT exchange their TO and E characters. It is important to note that this exchange was observed at a temperature close to room temperature. At 110 K, these branches of LT are of the same type as those of LN at room and low temperature [9]. This exchange is related to the important softening of the A_1(1TO) mode with temperature [13]. The frequency of the A_1(1TO) mode in LT becomes lower than the frequency of the E(2TO) mode close to room temperature while crossing of these modes takes place at around 700 °C in LN.

The mode dampings are dependent on the compositional disorder in the solid solutions. In LNT_x mixed crystals, dampings of the modes are affected by Li nonstoichiometry as well. Thus, to estimate the disorder effect on the phonons, LNT_x Czochralski-grown crystals were compared. The Raman spectra consist of relatively narrow spectral lines with a line width of the same order (increase by 2 - 6 cm^{-1}) as that in the pure LN and LT crystals, while the line shifts of some vibrational frequencies are large. This means that the broadening of the phonon distribution function caused by composition fluctuations is small.

The variation of the total intensity of unpolarized Raman spectra (collected using a 633 nm excitation and reduced by the Bose-Einstein distribution) of stoichiometric LNT_x powders as a function of Ta/(Ta+Nb) ratio is given in Fig. 9. Note that the total Raman intensity of Nb-rich solid solutions remains almost constant or even maybe slightly increases when Ta replaces Nb. In Ta-rich solid solutions, the intensity decreases with increase of Ta concentration. The total Raman efficiency of LN is higher by a factor of 2 compared with that of LT. The difference in total intensity of the polarized Raman spectra measured in LN and LT single crystals at different polarization configurations is represented in Fig. 9, as well. A lower total Raman efficiency of LT compared with that of LN was observed in all polarization configurations (Fig. 9). The

complete set of non-zero Raman tensor coefficients determining the activity of different E and A_1 phonon modes of LN and LT was estimated experimentally and is given in Table VII and Fig. 10. All the coefficients were normalized with respect to the d^2 coefficient of E(1TO) mode of LN. First, the integrated Raman tensor coefficients (the sum of the same type of coefficients representing particular modes) of LN and LT can be compared. This analysis of the overall intensity of E and A_1 modes, characterized by different coefficients, indicates that the d^2, c^2, c'^2, a^2 and a'^2 coefficients of LT are around three times lower than those of LN (Table VII) while the b^2 coefficient reduces by 50 % when Nb is completely replaced by Ta. The highest intensity of the Raman effect was observed in the $X(ZZ)\bar{X}$ polarization configuration in both end members (Fig. 10). In this polarization configuration, A_1(TO) modes are observed and their activity is described by the b^2 coefficient of the Raman tensor (Table I). The integrated b^2 coefficient ($b^2 = \sum_j {b_j}^2$, where b_j coefficients represent j^{th} modes) is more than three and five times higher than other non-zero Raman tensor coefficients of LN and LT, respectively (Table V). Therefore, the change of complete Raman intensity with Nb/Ta ratio in LN-LT powders is very similar to that of $X(ZZ)\bar{X}$ (or $Y(ZZ)\bar{Y}$) spectra (Fig. 9). The d^2/b^2 and a^2/b^2 coefficient ratios are similar in both materials. The integrated c^2 coefficient is very low in LN and LT. The intensities of longitudinal E and A_1 modes are represented by c'^2 and a'^2, respectively. The integrated coefficients c'^2 ($c'^2 = \sum_j c_j'^2$) and a'^2 ($a'^2 = \sum_j a_j'^2$) of LN and LT are lower than the integrated c^2 and a^2 coefficients describing the intensities of the transverse modes, respectively. The larger difference in total intensity of LO and TO modes was observed for the A_1-symmetry modes compared with that of the E modes in both end-members.

In general, the intensities of the individual Raman modes in LT are lower than those of the equivalent modes in LN with the exception of the E(9TO), E(8LO), E(5TO), E(4LO), A_1(3TO) and A_1(2LO) modes. The E(9TO) and E(8LO) modes present considerably higher efficiency in LT than in LN, while the A_1(3TO) and A_1(2LO) modes have very close absolute intensities in both materials. The E(5TO) and E(4LO) modes have extremely low Raman efficiency in both materials. It is important to note that the eigenvectors of the E(9TO)- E(8LO) and A_1(3TO) - A_1(2LO) mode pairs present strong overlapping and these mode pairs have very little overlap with other modes. The E(6TO)-E(5LO) and A_1(2TO)-A_1(2LO) modes with singularly overlapped eigenvectors present decreased intensities in LT in comparison with those in LN. All other remaining modes E(TO)-E(LO) and A_1(TO)-A_1(LO) modes (the group of E(1TO)- E(5TO), E(7TO) & E(8TO) modes with E(1LO)- E(4LO), E(6LO), E(7LO) & E(9LO) modes and the

group of A_1(2TO) & A_1(4TO) with A_1(3LO) & A_1(4LO)) present a network interaction and the intensities of all these modes decrease when Nb is replaced by Ta. This analysis indicates that if the intensities of particular TO modes decrease when one element is replaced by another element in the solid solutions, then the intensities of LO modes strongly overlapped with these TO modes will decrease as well. Thus, overlapping of eigenvectors of the LO-TO modes is a also good criterion for the prediction of the change in intensities of LO (or TO) modes in mixed-systems.

In both LN and LT, the c'^2 and a'^2 coefficients are lower than the c^2 and a^2 coefficients, respectively: and this decrease in the intensities of the LO modes is related to the electro-optic coupling (see discussion for more details). However, comparison of the intensities of (TO) and (LO) individual modes is not straightforward, as the $c_j'^2$ and $a_j'^2$ coefficients of j^{th} mode are not always smaller than the c_j^2 and a_j^2 coefficients of the same j^{th} mode (Table VII). This is the case for the 3rd, 5th, 6th, 9th E(LO) modes and the 3rd A_1(LO) mode of LN and the 3rd, 5th, 9th E(LO) modes and the 2nd A_1(LO) mode of LT, which have higher Raman efficiencies than those of the equivalent j^{th} (TO) modes (Table VII). Therefore, we calculated effective $c_j^{eff^2}$ and $a_j^{eff^2}$ coefficients for each j^{th} LO mode taking into account the overlap of eigenvectors from

$$a_j^{eff^2} = \sum_i o_{ij} a_i^2 \quad and \quad c_j^{eff^2} = \sum_i o_{ij}\, c_i^2 \tag{8}$$

Where o_{ij} – the overlap coefficient between eigenvectors of i^{th} TO and j^{th} LO modes, c_i^2 and a_i^2– the coefficients of the Raman tensor of the i^{th} TO mode. These effective coefficients take into account the overlap eigenvectors of LO modes with several TO modes. The estimated $c_j^{eff^2}$ and $a_j^{eff^2}$ coefficients are given in Table VII. The $a_j^{eff^2}$ and $c_j^{eff^2}$ coefficients have values higher than or equal to those of the $a_j'^2$ and $c_j'^2$ coefficients of the j^{th} mode in both LN and LT. This confirms that the Raman efficiencies of all LO modes tend to decrease with respect to the intensity of TO modes as a result of the effect of electro-optic couplings.

Discussion

LNT_x solid solutions present one-mode behaviour indicating that the mass and/or force constant changes due to substitution of Nb by Ta are not large enough to result in splitting of the vibrational states of the local modes. At wavenumbers lower than 325 cm^{-1}, the wavenumbers of all A_1 and E modes decrease with increase of Ta concentration within LNT_x (see Fig.6, Tables II, III and IV). This can be explained by the change of atomic masses: the replacement of Nb by

a heavier atom, such as Ta. This affects especially vibrations at low wavenumbers in which heavy atoms like Nb and Ta are highly involved. However, this simple criterion is not sufficient to explain the behaviour of modes with wavenumbers higher than 325 cm^{-1} for the LN-LT mixed system. This indicates that the changes in force constants are important in this system, as well. Thus, changes in long-range force constants resulting from variations of the effective charge ought to be taken into account [20]. Effective charges of transverse optical modes of LN were reported by Hermet *et al*. [17]. and higher average effective charges in LT compared with those in LN were found by Gervais [34]. The frequencies of most of the modes at high-wavenumbers (> 325 cm^{-1}) increase with the increase of Ta/Nb ratio as a consequence of enhanced force constants. The increase of the long-range electrostatic forces with the replacement of Nb by Ta was also indicated by the transformation of two oblique mode branches with A- and E- symmetry to LO and TO branches at intermediate wavenumbers (333-373 cm^{-1}) in the case of Ta-rich solid solutions. However, the exceptions to these rules are the E(4LO), E(9LO), A_1(3LO), A_1(4LO) and A_1(4TO) modes (Fig. 6). The change of frequencies of these modes as a function of Ta/Nb ratio can be explained by calculating the weighted shift (Eq. 4) which takes into account the interdependence (overlap of eigenvectors) of modes (Fig. 7).

DFT theory could predict the effect of Ta/Nb composition on the frequencies of the most E(TO) and A_1(TO) modes of LNT_x crystals [24]. However, the shift of frequencies of A_1(2TO), E(1TO), E(3TO) and E(4TO) modes with Ta/Nb composition, measured experimentally, presented opposite trends to those predicted by DFT simulations and the authors have attributed this deviation from theoretical results to the Li nonstoichiometry of LNT_x crystals [24]. In this work, LNT_x crystals with different Ta/Nb ratios had different Li concentrations: $LNT_{0.18}$, $LNT_{0.3}$ and $LNT_{0.43}$ had Li concentration close to the congruent compositions of the end members and $LNT_{0.67}$ was nearly stoichiometric [32]. The comparison of A_1(TO), A_1(LO), E(LO) and E(TO) mode frequencies of congruent and stoichiometric LN and LT specimens was reported by Margueron et al. [9]. The increase of Li defect concentration by 2 mol% results in a shift of an order of 1 cm^{-1} of modes to lower wavenumbers. In LNT_x, the *x* composition parameter varies from 0 to 1 and the errors in the estimation of *x* and the wavenumbers of the Raman modes were 0.01 and 0.5 cm^{-1}, respectively. Thus, the influence of the Li concentration on the change of mode wavenumbers with Ta/Nb ratio can be neglected in our work and in the literature data and the mass and/or force constant changes and the overlap of mode eigenvectors are sufficient to interpret completely compositional dependence of Raman mode shifts in LN-LT solid solutions.

Nevertheless, the change in the dampings with Li concentration is considerable and must be taken into account in an analysis of disorder effects in the mixed crystals [26]. The broadening of the phonon distribution function caused by composition fluctuations is small in the case of mixed LN-LT crystals as the width of their spectral lines was of the same order as that in the end members.

In order to analyse the Raman efficiency, we consider the Stokes scattering efficiency, $S_{ij,k}$, which depends on the electro-optic coefficients, r_{ij}, and is given by [35]

$$S_{ij,k}(TO) = D(TO)\left|\alpha_{ij,k}\right|^2, \quad (5)$$

$$S_{ij,k}(LO) = D(LO)\left|\alpha_{ij,k} + \xi_{ij,k}/\beta_{kk}\right|^2, \text{ and} \quad (6)$$

$$D(TO,LO) = \frac{\hbar\omega_s^4(\bar{n}_{TO,LO}+1)vLd\Omega}{32\pi^2c^4\bar{m}\omega_{TO,LO}} \quad (7)$$

where $\alpha_{ij,k}$ stands for the coefficient of the polarizability tensor (Raman tensor) or a deformation of the electron potential function due to a change in a lattice spacing, i, j and k represents the directions in the orthogonal settings, $\xi_{ij,k}$ and β_{kk} are deformations of the electron potential function and lattice spacing by the direct action of the electric field, respectively. The β_{kk} is proportional to the infrared strength. $D(TO,LO)$ are cross section coefficients dependent on geometry, temperature and wavelength. The ω_s^4 term is the Rayleigh intensity dependence on laser scattering wavelength, $(\bar{n}_{TO,LO}+1)$ - the Bose factor, $\bar{m}$ - the reduce mass of the unit cell volume, v. The particular intensities of the modes depend on their partial polarization. The coefficients of Raman and electro-optic tensors, describing the intensities of A_1- and E-symmetry phonons in different polarization configurations, are summarized in Table VIII. The electro-optic coefficients, measured at 633 nm, of LN and LT are also given in Table VIII. In fact, in polar LN and LT, the modulation of the light intensity (electro-optic properties) can be determined from IR and Raman intensities as discussed by Kaminow et al. [25] The c'^2 and a'^2 coefficients of Raman tensor are related to the electro-optic coupling. Thus, c'^2 (a'^2) and c'^2/c^2 (a'^2/a^2) ratio can be used as factors giving information about the electro-optic performance of materials. The integrated c'^2 and a'^2 coefficients of LN are higher by a factor of 3 compared with c'^2 and a'^2 of LT (Table VIII), respectively. This shows that LN presents stronger electro-optic coefficients. This estimate is in a good agreement with the results obtained by means of a THz rectifying process, which involved only the contribution of lattice dynamics to the electro-optic

properties [36]. LT has the same r_{32} electro-optic coefficient as LN, while its r_{13} is slightly lower than that of LN. This may explain the smaller difference in b^2 coefficients than in a^2 coefficients of LT and LN (Table VIII). Using similar reasoning, we would expect more significant change in intensities of E-modes related to the c^2 coefficient than in those defined by the d^2 coefficient when Ta replaces Nb, because of the very different r_{22} and quite similar r_{51} coefficients of LN and LT. However, the difference in c^2 coefficients of the end members is less pronounced than that in the d^2 coefficients. This indicates that the difference in the electro-optic coefficients of LN and LT is not due to the change in Raman efficiency when Ta replaces Nb. Thus, perturbation theory on its own is not sufficient to describe the variations of Raman intensity in the LN-LT system.

In fact, LN presents a smaller gap (~ 3.87 eV) than LT (~ 4.77 eV). This results in higher refractive indices of LN (n_o(LN) = 2.288, n_e(LN) = 2.203) compared with those of LT (n_o(LT) = 2.179, n_e(LT) = 2.182). The difference in gap of LN and LT can introduce some difference in Raman efficiency even far from resonance conditions. The higher refraction index of LN with respect to that of LT results in the increased Raman scattering efficiency due to scattered volume correction of 7 % (calculated using Fresnel law for transmission) and local field correction [37] of 10 %. This would only partially explain the higher Raman intensity of LN than that of LT.

Furthermore, the Raman efficiency is highly related to the ionicity/covalency of the bonds in these materials. Inbar and Cohen studied theoretically the similarities/differences in the electronic structure and energetics of LN and LT, but they did not find a significant difference in their ionicity/covalency [38]. Although the significantly higher melting point (1650 °C (LT) and 1257 °C (LN)) and much lower Curie temperature (603 °C (congruent LT) and 1142 °C (congruent LN)) of LT, as compared with those of LN, would suggest a more pronounced ionic character of bonds in LT than in LN [14]. So far these differences in properties of isostructural LN and LT have not been explained theoretically. As indicated above, the increase of long-range force constants and the effective charges in LT with respect to those in LN were observed through the increase of mode wavenumbers at high frequencies and the change of the character of two oblique mode branches. The increased effective charges can be attributed to the increased ionicity of the bonds in LT. The reflectivity, measured by IR spectroscopy (Fig. 5), indicated the increase of dipolar strength when Nb is replaced by Ta, as well. These results are in a good agreement with IR data for end members, reported by Gervais [34]. Thus, most of the E- and A_1-symmetry modes of LT present lower Raman intensities compared with those of LN also due to higher

ionicity of LT bonds. The change of intensities of particular LO and TO modes was related to their network interaction (overlap of eigenvectors).

Lattice dielectric constants of both end members have been calculated previously using the Lyddane-Sachs-Teller relation [9]. The amplitude and anisotropy mainly arise from low-frequency modes [27]. The lattice dielectric constant of mixed LNT_x crystals changes continuously when Ta replaces Nb as TO and LO modes continuously shift as a function of Ta/Nb composition. Thus, the strong THz anisotropy of LN can be tuned by partially replacing the Nb by Ta. This makes the LNTx solid solutions an interesting system for THz component applications.

Concluding remarks

The wavenumbers of all 27 optical phonons at the Γ point of LN, LT and LNT_x single crystals were determined experimentally using Raman and IR spectroscopies. The overlap matrix of TO-LO phonons and the directional dispersion branches of extraordinary phonons were calculated. Absolute values of non-zero Raman tensor coefficients determining the activity of phonon modes of LN and LT were determined experimentally. The dynamical properties of the mixed crystals are highly dependent on the Nb and Ta composition. The effect of compositional disorder in LNT_x crystals is small, resulting in a small deviation from Vegard's law and damping of the phonons comparable with those of the end-members. At low frequencies the wavenumbers of phonon modes decrease continuously on replacing Nb by Ta as a result of the atomic mass effect. The frequencies of most of the high-frequency modes increase with the Ta/Nb ratio owing to enhanced force constants. There is however some exception for the modes with eigenvectors overlapping with the low-frequency modes. The Raman efficiency decreases by several orders when Ta replaces Nb. It was shown that the Raman intensities of LO and TO modes are also related through the overlap matrix. The analysis of the overlap matrix of eigenvectors of LO-TO phonons allows one to predict the signs of changes in intensity and frequency of LO or TO phonons in solid solution systems.

Acknowledgements

Authors would like to thank Dr. J. Hlinka for the valuable discussions on the topic. We are grateful to the Engineering and Physical Sciences Research Council (EPSRC) for a grant that enabled this work to be carried out. This work was also supported by the Czech Science

Foundation (Project GACR P204/10/0616), by KAN 301370701 project of the Academy of Sciences of the Czech Republic and French National Research Agency fundings EUR EIPHI program grant number ANR-17-EURE-0002, ANR LiLit grant number ANR-16-CE24-0022-011 and ANR JCJC LiLa ANR-12-JS04-0008-01.

Tables

Table I Polarization configurations in standard Porto's notation and corresponding coefficients of the Raman tensor and fitting parameters of Raman spectra. (X,Y,Z) is an orthogonal reference system where Z- and X-axes are parallel to the crystallographic c- and a-axes in hexagonal setting, respectively, the a-axis is taken to be perpendicular to the mirror plane of the 3m point group.

Modes	*Coefficient*	*Polarization configuration*	*Conditions of fitting*
E(TO)	*d*	$X(ZY)\bar{X}$, $Y(ZX)\bar{Y}$	*No fixed parameters, intensity was corrected by using Eq.1*
	c	$Z(XY)\bar{Z}$	*No fixed parameters, intensity was corrected by using Eq.1*
A_1(TO)	*a*	$X(YY)\bar{X}$	*Fixed wavenumbers, dampings and intensities of E(TO) modes, estimated from $Z(XY)\bar{Z}$ spectra. The effect of change from VH to VV polarization configuration on intensity was corrected by using Eq.1*
	b	$Y(ZZ)\bar{Y}$, $X(ZZ)\bar{X}$	*No fixed parameters, intensity was corrected by using Eq.1*
A_1(LO)	*a'*	$Z(XX)\bar{Z}$	*Fixed wavenumbers, dampings and intensities of E(TO) modes, estimated from $Z(XY)\bar{Z}$ spectra. The effect of change from VH to VV polarization configuration on intensity was corrected by using Eq.1*
E(LO)	*c'*	$Y(XX)\bar{Y}$	*Fixed wavenumbers, dampings and intensities of A_1(TO) modes, estimated from $X(YY)\bar{X}$ spectra, intensity was corrected by using Eq.1*

Table II Wavenumbers of A_1(TO)and A_1(LO) modes of LNT_x crystals with different x.

	1TO	2TO	3TO	4TO	1LO	2LO	3LO	4LO
CLN	253	276	333	632	275	333	418	871
$LNT_{0.18}$	247	273	335	627	272	335	421	870
$LNT_{0.31}$	244	271	337	624	270	337	421	870
$LNT_{0.43}$	239	268	340	619	267	340	418	868
$LNT_{0.67}$	225	264	351	609	264	349	415	866
CLT	207	256	357	598	256	355	405	865

Table III Wavenumbers of E(TO) modes of LNT_x crystals, estimated from Raman (RS) and IR spectra.

		1TO	2TO	3TO	4TO	5TO	6TO	7TO	8TO	9TO
CLN	RS	154	238	265	322	-	370	433	579	~660
	IR	152	235	260	322	358	-	432	577	667
$LNT_{0.18}$	RS	152	234	263	321	-	372	436	579	660
	IR	152	232	258	322	361	-	439	577	667
$LNT_{0.31}$	RS	152	232	263	321	-	373	439	580	660
	IR	150	232	258	320	361	-	439	579	667
$LNT_{0.43}$	RS	151	227	261	321	-	375	442	581	657
	IR	150	225	258	320	364	-	445	581	666
$LNT_{0.67}$	RS	146	220	256	319	-	379	453	586	660
	IR	143	222	253	318	368	-	451	586	664
CLT	RS	144	209	253	316	-	383	464	591	659
	IR	142	-	253	315	373	-	462	592	663

Table IV Wavenumbers of E(LO) modes, determined from IR and Raman spectra (RS).

	CLN		$LNT_{0.18}$	$LNT_{0.31}$	$LNT_{0.43}$	$LNT_{0.67}$	CLT	
	RS	IR spectroscopy						RS
1LO	194	196	196	196	196	196	194	194
2LO	239	239	237	237	228	228	-	211*
3LO	297	294	291	291	289	286	280	280
4LO	-	343	343	343	343	344	344	-
5LO	370	-	-	-	-	-	-	383
6LO	425	426	431	432	439	443	453	454
7LO	457	452	457	457	463	468	475	472*
8LO	-	659	661	659	662	663	662	659
9LO	878	876	876	876	876	868	865	864

Table V Overlap matrix between eigenvectors of the A_1(LO) and A_1(TO) modes of LN and LT.

	1LO	2LO	3LO	4LO
		$LiNbO_3$		
1TO	0.219	0	**0.868**	0.446
2TO	**-0.976**	0	0.198	0.092
3TO	0	**1**	0	0
4TO	-0.008	0	-0.455	**0.890**
		$LiTaO_3$		
1TO	0	0.294	**-0.815**	0.500
2TO	**1**	0	0	0
3TO	0	**-0.951**	-0.303	0.064
4TO	0	-0.100	0.494	**0.864**

Table VI Overlap matrix between eigenvectors of the E(LO) and E(TO) modes of LN and LT.

	1LO	2LO	3LO	4LO	5LO	6LO	7LO	8LO	9LO
					$LiNbO_3$				
1TO	**0.868**	-0.069	-0.204	-0.120	0	0.155	-0.253	-0.053	0.307
2TO	-0.152	**-0.979**	-0.085	-0.038	0	0.040	-0.062	-0.012	0.065
3TO	-0.428	0.186	**-0.688**	-0.230	0	0.213	-0.326	-0.058	0.317
4TO	-0.153	0.037	**0.643**	**-0.584**	0	0.229	-0.322	-0.048	0.249
5TO	-0.109	0.024	0.239	**0.764**	0	0.331	-0.413	-0.051	0.255
6TO	0	0	0	0	**1**	0	0	0	0
7TO	-0.022	0.004	0.032	0.038	0	**-0.846**	-0.522	-0.021	0.094
8TO	-0.065	0.012	0.076	0.073	0	-0.222	0.521	-0.318	**0.750**
9TO	-0.015	0.003	0.017	0.016	0	-0.042	0.090	**0.942**	0.320
					$LiTaO_3$				
1TO	**-0.840**	-0.172	0.247	0.166	0	0.193	-0.202	0	0.315
2TO	0.238	**-0.969**	0.041	0.022	0	0.022	-0.023	0	0.032
3TO	0.431	0.161	**0.763**	0.236	0	0.199	-0.202	0	0.264
4TO	0.181	0.057	**-0.552**	**0.674**	0	0.259	-0.253	0	0.272
5TO	0.124	0.037	-0.211	**-0.672**	0	0.461	-0.411	0	0.325
6TO	0	0	0	0	**1**	0	0	0	0
7TO	0.015	0.004	-0.020	-0.031	0	**-0.724**	**-0.684**	0	0.080
8TO	0.065	0.019	-0.075	-0.097	0	-0.345	0.466	0	**0.803**
9TO	0	0	0	0	0	0	0	**1**	0

*Table VII Non-zero Raman tensor coefficients determining Raman efficiency of phonon modes of LN and LT crystals. The coefficients of LT which are equal or higher to those of LN are indicated in **bold** script.*

	$LiNbO_3$				$LiTaO_3$			
E modes	d_j^2	c_j^2	c'^2_j	$c_j^{eff^2}$	d_j^2	c_j^2	c'^2_j	$c_j^{eff^2}$
1	1	0.18	0.03	0.2	0.34	0.019	0.016	0.04
2	0.91	0.08	0.05	0.1	0.22	0.014	0.005	0.02
3	0.24	0.05	0.17	0.2	0.02	0.010	0.024	0.04
4	0.69	0.09	*	0.1	0.32	0.042	*	0.04
5	*	*	0.16	0.2	*	*	0.043	0.09
6	0.53	0.15	0.27	0.3	0.32	0.094	0.093	0.09
7	0.19	0.18	0.03	0.3	0.05	0.082	0.005	0.09
8	1.48	0.27	*	0.1	0.27	0.034	**0.035**	0.08
9	*	*	0.23	0.3	**0.10**	**0.075**	0.062	0.06
$\sum_j \alpha_j$	5.04	1.00	0.94		1.64	0.37	0.28	
A_1 modes	a_j^2	b_j^2	a'^2_j	$a_j^{eff^2}$	a_j^2	b_j^2	a'^2_j	$a_j^{eff^2}$
1	0.67	7.51	0.31	0.5	0.22	5.33	0.085	0.1
2	0.41	2.47	0.26	0.3	0.10	0.71	**0.23**	0.4
3	0.32	0.14	0.56	2.4	**0.31**	**0.11**	0.14	0.7
4	3.91	8.52	1.88	3.8	0.78	2.98	0.41	0.8
$\sum_j \alpha_j$	5.31	18.64	3.01		1.41	9.13	0.87	

**too low intensity*

Table VIII Relation between the electro-optic coefficients, r_{ij}, and non-zero Raman tensor coefficients, α_{ijk} , determining Raman efficiency of phonon modes of LN and LT crystals in different polarization configurations. The ratios of experimentally estimated Raman coefficients and electro-optic coefficients of LT and LN are given for comparison.

Modes	Pol.conf.*	α_{ijk}	$\frac{\sum_j \alpha_j{}^2(LT)}{\sum_j \alpha_j{}^2(LN)}$	r_{ij} (pm/V)	$\frac{r_{ij}(LT)}{r_{ij}(LN)}$
A_1-symmetry modes with translation along Z-axis					
TO	$Y(XX)\bar{Y}$ $X(YY)\bar{X}$	a=α_{xx}=α_{yy}=α_{111}= =α_{222}	$\frac{\sum_j a_j^2(LT)}{\sum_j a_j^2(LN)} = 0.26$	$\sim r_{13}$	$\sim \frac{8}{10} = 0.8$
TO	$X(ZZ)\bar{X}$ $Y(ZZ)\bar{Y}$	b=α_{zz}=α_{333}	$\frac{\sum_j b_j^2(LT)}{\sum_j b_j^2(LN)} = 0.49$	$\sim r_{33}$	$\sim \frac{33}{33} = 1$
LO	$Z(XX)\bar{Z}$ $Z(YY)\bar{Z}$	a'=α_{xx}'=α_{yy}'= =α_{111}+ ξ_{111}/ β_{11} =α_{222}+ ξ_{222}/ β_{22}	$\frac{\sum_j a'^2_j(LT)}{\sum_j a'^2_j(LN)} = 0.29$	$\sim r_{13} + e$	-
E-symmetry modes with translation in the X-Y plane					
TO	$Z(XY)\bar{Z}$ $Z(YX)\bar{Z}$	c=α_{xy}=α_{112}=α_{yx}= α_{112}=α_{221}	$\frac{\sum_j c_j^2(LT)}{\sum_j c_j^2(LN)} = 0.37$	$\sim r_{22}$	$\sim \frac{1}{7} = 0.14$
TO	$X(YZ)\bar{X}$ $X(ZY)\bar{X}$	d=α_{yz}=α_{zy}=α_{223}= =α_{332}	$\frac{\sum_j d_j^2(LT)}{\sum_j d_j^2(LN)} = 0.33$	$\sim r_{51}$	$\sim \frac{20}{28} = 0.71$
LO	$Y(XX)\bar{Y}$	c'=α_{xx}'= =α_{111}+ ξ_{111}/ β_{11}	$\frac{\sum_j c'^2_j(LT)}{\sum_j c'^2_j(LT)} = 0.30$	$\sim r_{22} + e$	-

Phonon-photon polarization configuration

Figure captions

Fig. 1 Unpolarized Raman spectra of stoichiometric LNTx powders with different x.

Fig. 2 Raman spectra, measured in $X(ZZ)\bar{X}$ or $Y(ZZ)\bar{Y}$ polarization configuration, of X- or Y-cut LNT_x crystals with different x. The area of the spectra was normalized to 1.

Fig. 3 Raman spectra, measured in $Z(XX)\bar{Z}$ or $Z(YY)\bar{Z}$ polarization configuration, of Z-cut LNT_x crystals with different x. The area of the spectra was normalized to 1.

Fig. 4 Comparison of E(TO) mode intensities in $Z(XY)\bar{Z}$ and $X(ZY)\bar{X}$/$Y(ZX)\bar{Y}$ spectra of Z-cut and X-cut LNT_x crystals with different x.

Fig. 5 Unpolarized near-normal reflectivity spectra $R(\omega)$, measured at RT, of Z-cut LNT_x crystals with different x.

Fig. 6 The change of E(TO), E(LO), A_1(LO) and A_1(TO) wavenumbers with the Ta/Nb ratio in LNT_x single crystals.

Fig. 7 Schematic representation of overlap between eigenvectors of TO and LO modes in LN (Overlap integrals from Table V and VI). The shift weights of mode are presented. The wavenumber of LN and LT are given in parenthesis (ω(LN)-ω(LT)). The arrows indicate if the frequency is increasing or decreasing when Ta replaces Nb. The red and blue lines show the main overlaps of the modes shifting to the higher and to the lower wavenumbers with the increasing Ta/(Ta+Nb) ratio, respectively. Blue zone indicates the low-frequency (< 325 cm^{-1}) zone and the orange color- high frequency zone (> 325 cm^{-1}).

Fig. 8 Directional dispersion branches of extraordinary phonons of LN, $LNT_{0.43}$ and LT. Θ is the angle between the c-axis and the phonon wave vector.

Fig. 9 The change of the total intensity of unpolarized Raman spectra with the Ta/Nb ratio in stoichiometric LNT_x powders. The integrated intensities of $Z(XX)\bar{Z}$, $Z(XY)\bar{Z}$, $X(YY)\bar{X}$, $X(YZ)\bar{X}$ and $X(ZZ)\bar{X}$ spectra of LN and L single crystals are given for comparison.

Fig. 10 Comparison of non-zero Raman tensor coefficients, α_j^2 , determining Raman efficiency of phonon modes of LN and LT crystals.

Figures

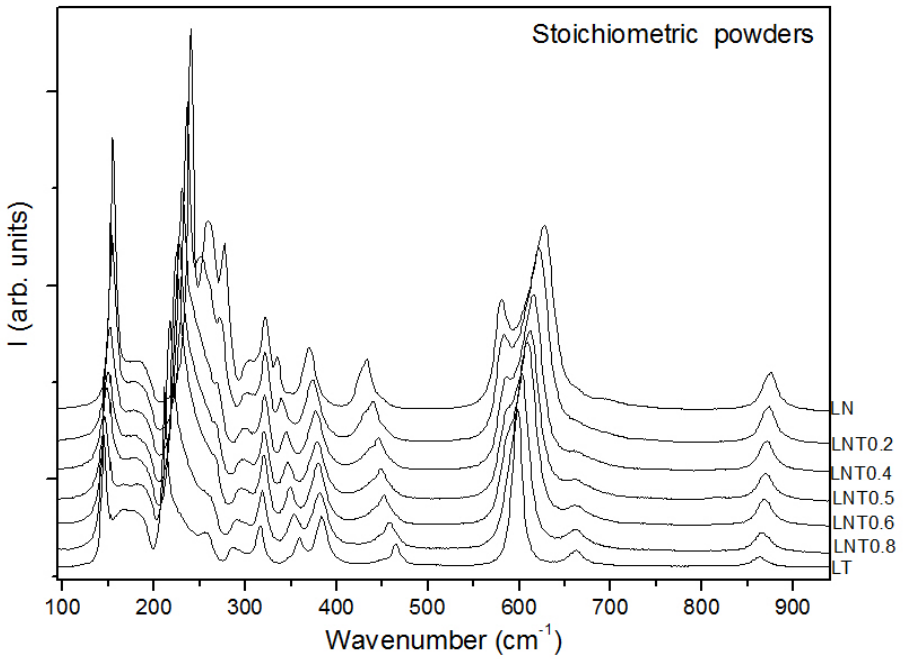

Fig. 1 Unpolarized Raman spectra of stoichiometric LNT_x powders with different x.

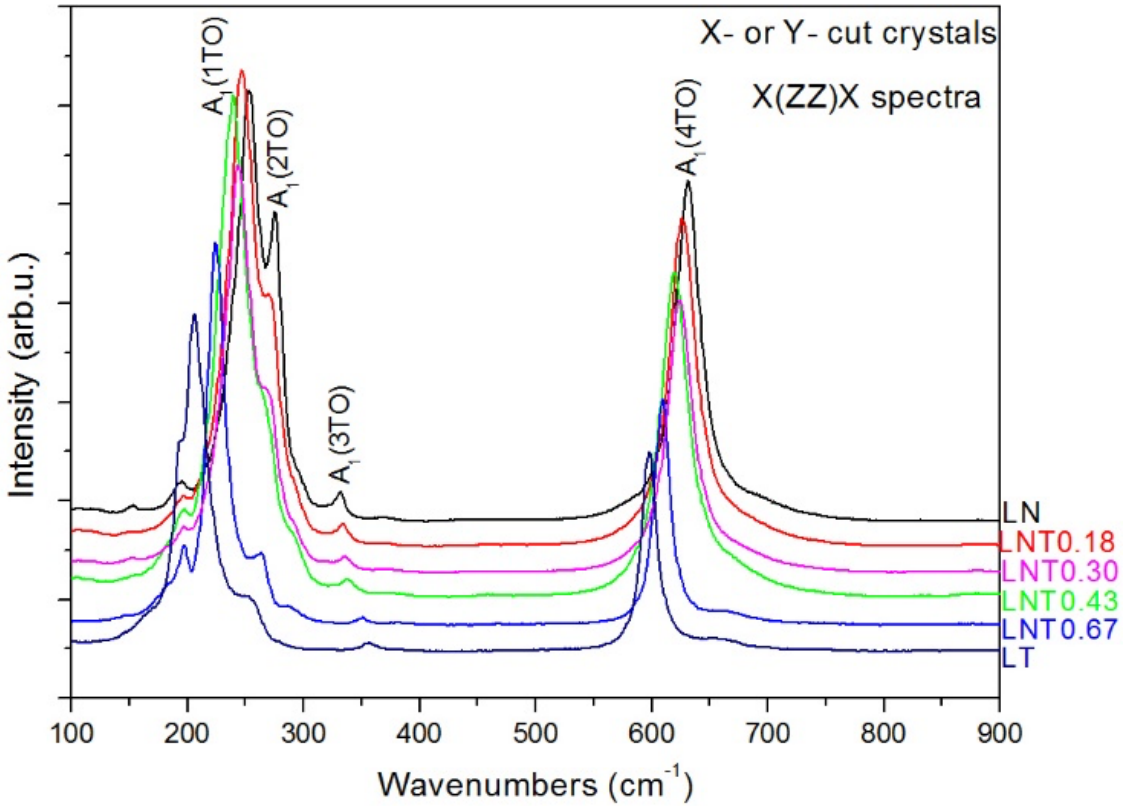

Fig. 2 Raman spectra, measured in $X(ZZ)\bar{X}$ or $Y(ZZ)\bar{Y}$ polarization configuration, of X- or Y-cut LNT_x crystals with different x.

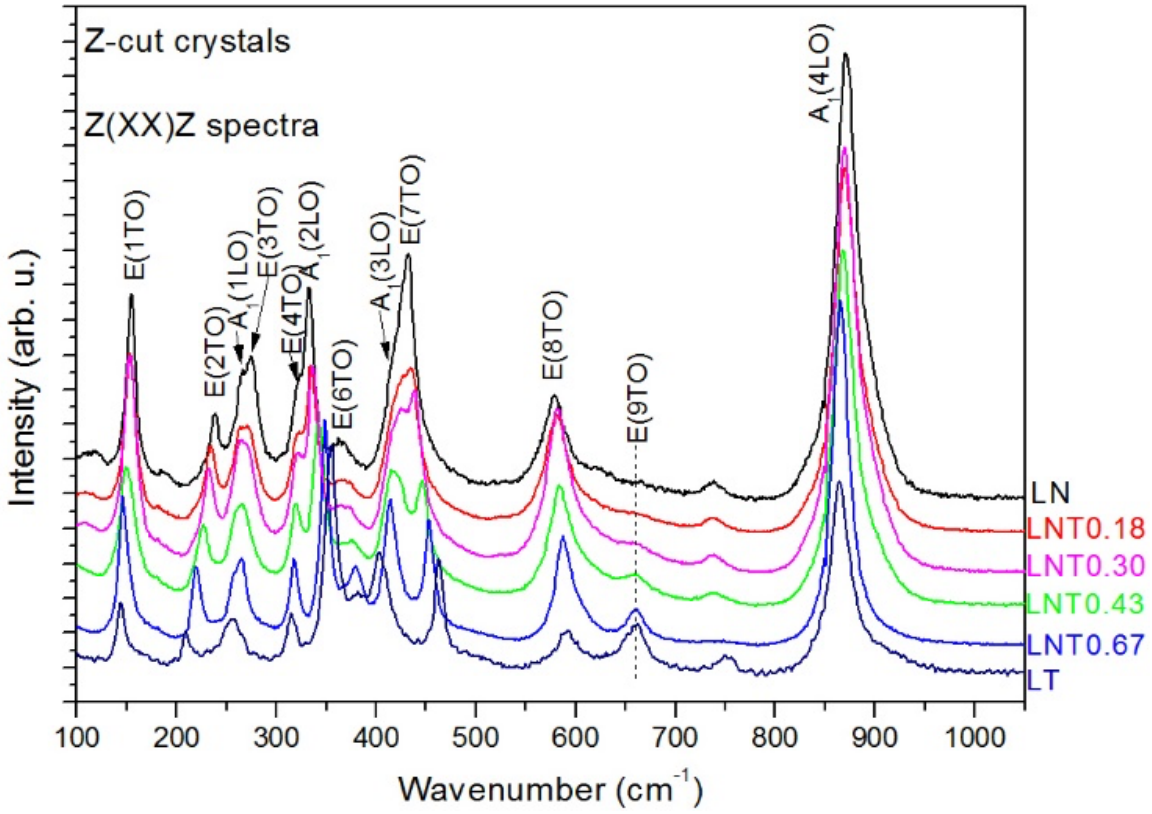

Fig. 3 Raman spectra, measured in $Z(XX)\bar{Z}$ or $Z(YY)\bar{Z}$ polarization configuration, of Z-cut LNT_x crystals with different x.

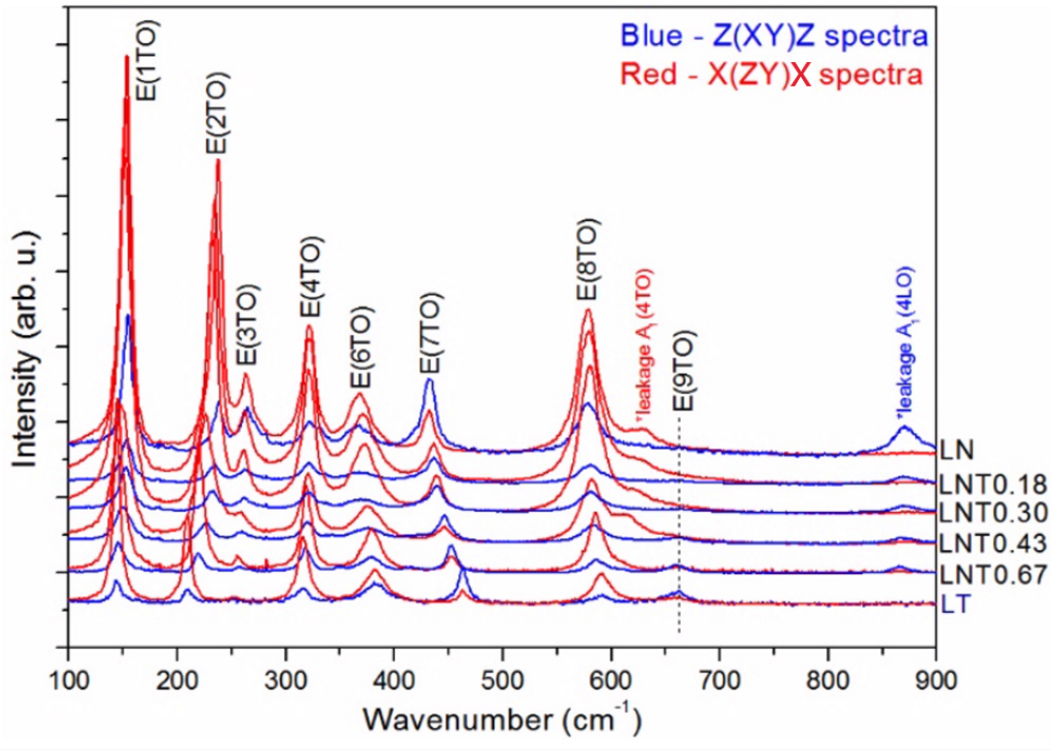

Fig. 4 Comparison of E(TO) mode intensities in $Z(XY)\bar{Z}$ and $X(ZY)\bar{X}/Y(ZX)\bar{Y}$ spectra of Z-cut and X-cut LNT_x crystals with different x.

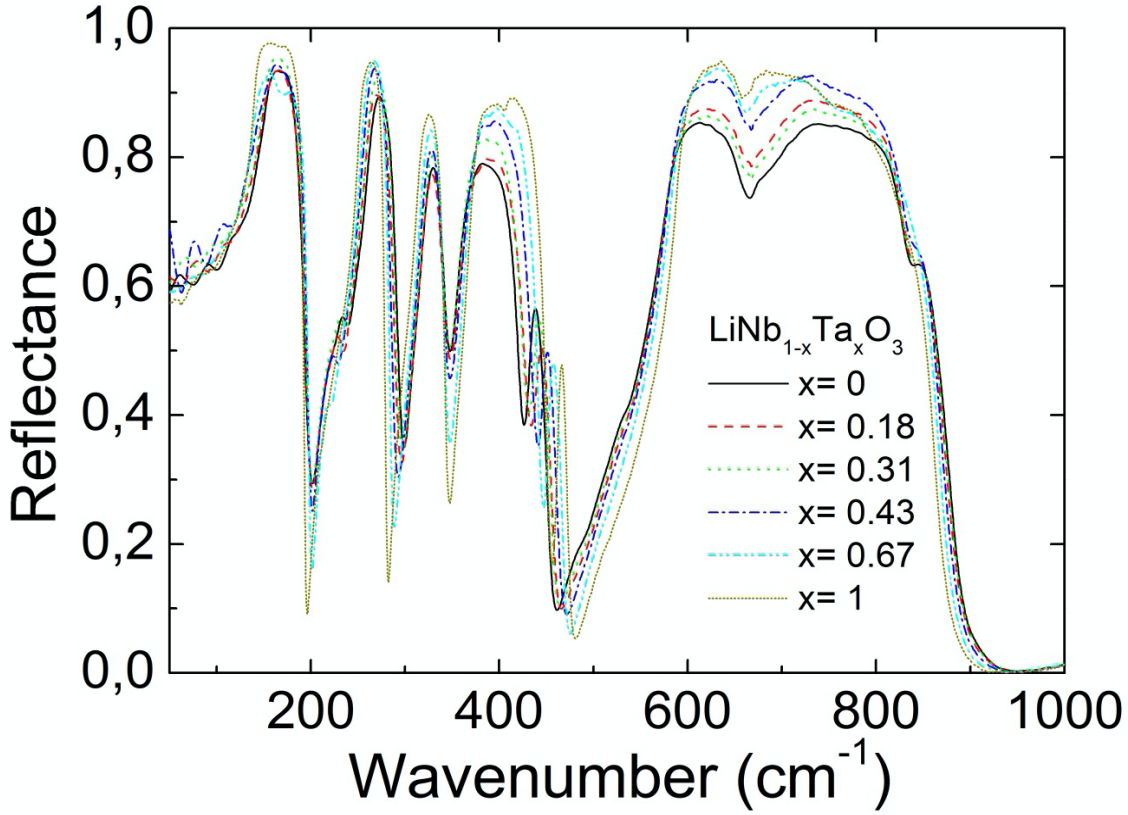

Fig. 5 Unpolarized near-normal reflectivity spectra $R(\omega)$, measured at RT, of Z-cut LNT_x crystals with different x.

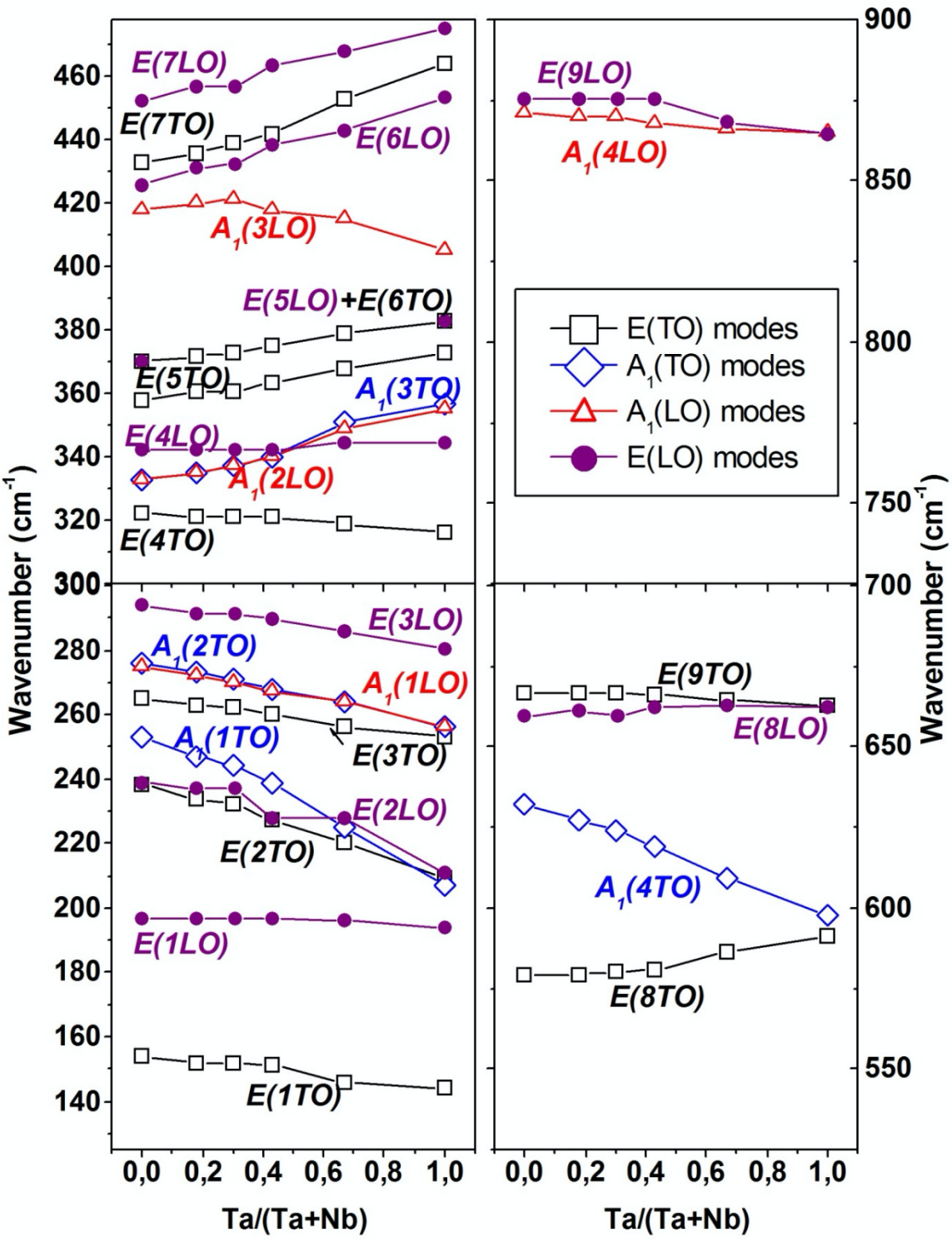

Fig. 6 The change of E(TO), E(LO), A_1(LO) and A_1(TO) wavenumbers with the Ta/Nb ratio in LNT_x single crystals.

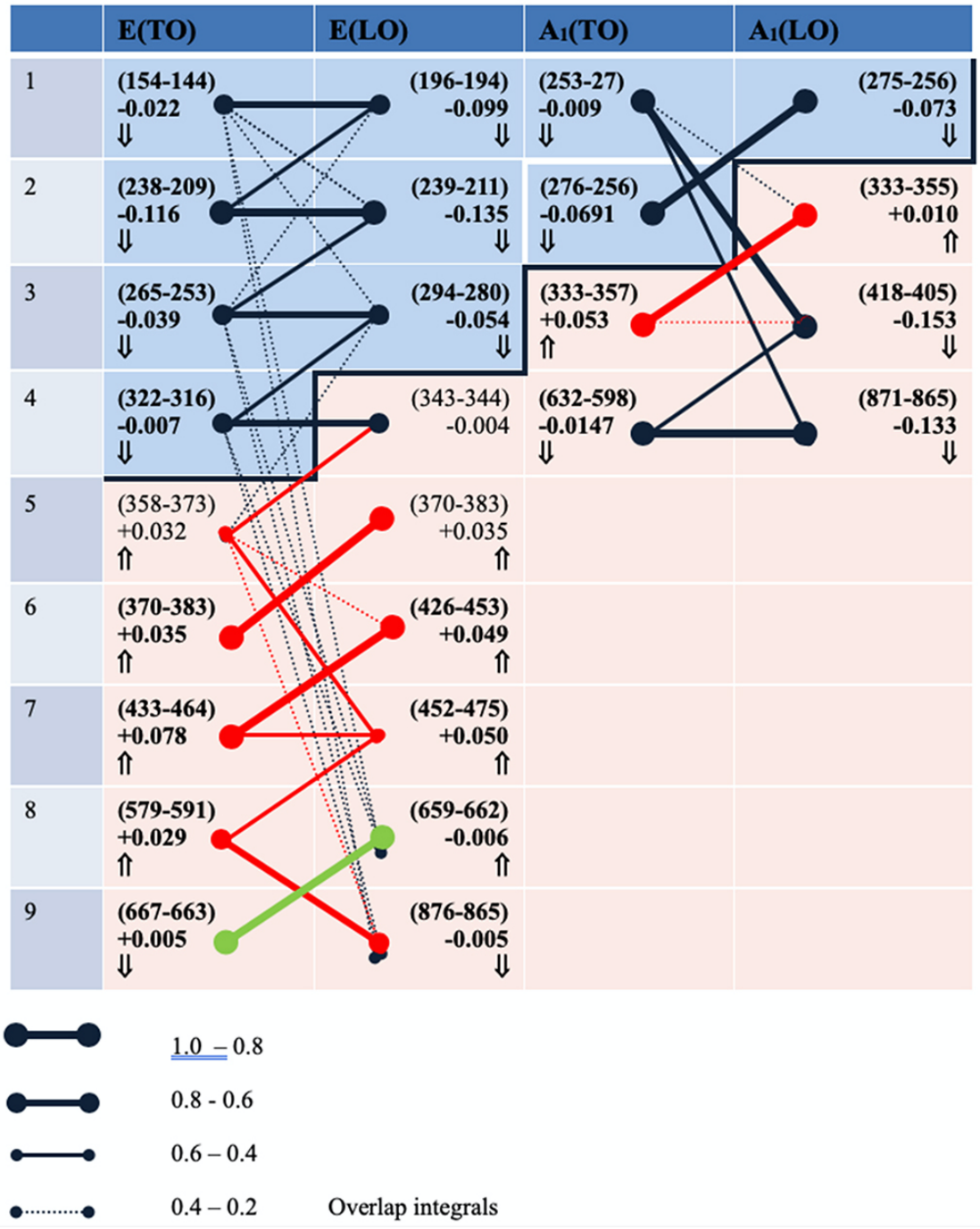

Fig. 7 Schematic representation of overlap between eigenvectors of TO and LO modes in LN (Overlap integrals from Table V and VI). The shift weights of mode are presented. The wavenumber of LN and LT are given in parenthesis (ω(LN)-ω(LT)). The arrows indicate if the frequency is increasing or decreasing when Ta replaces Nb. The red and blue lines show the main overlaps of the modes shifting to the higher and to the lower wavenumbers with the increasing Ta/(Ta+Nb) ratio, respectively. Blue zone indicates the low-frequency (< 325 cm^{-1}) zone and the orange color- high frequency zone (> 325 cm^{-1}).

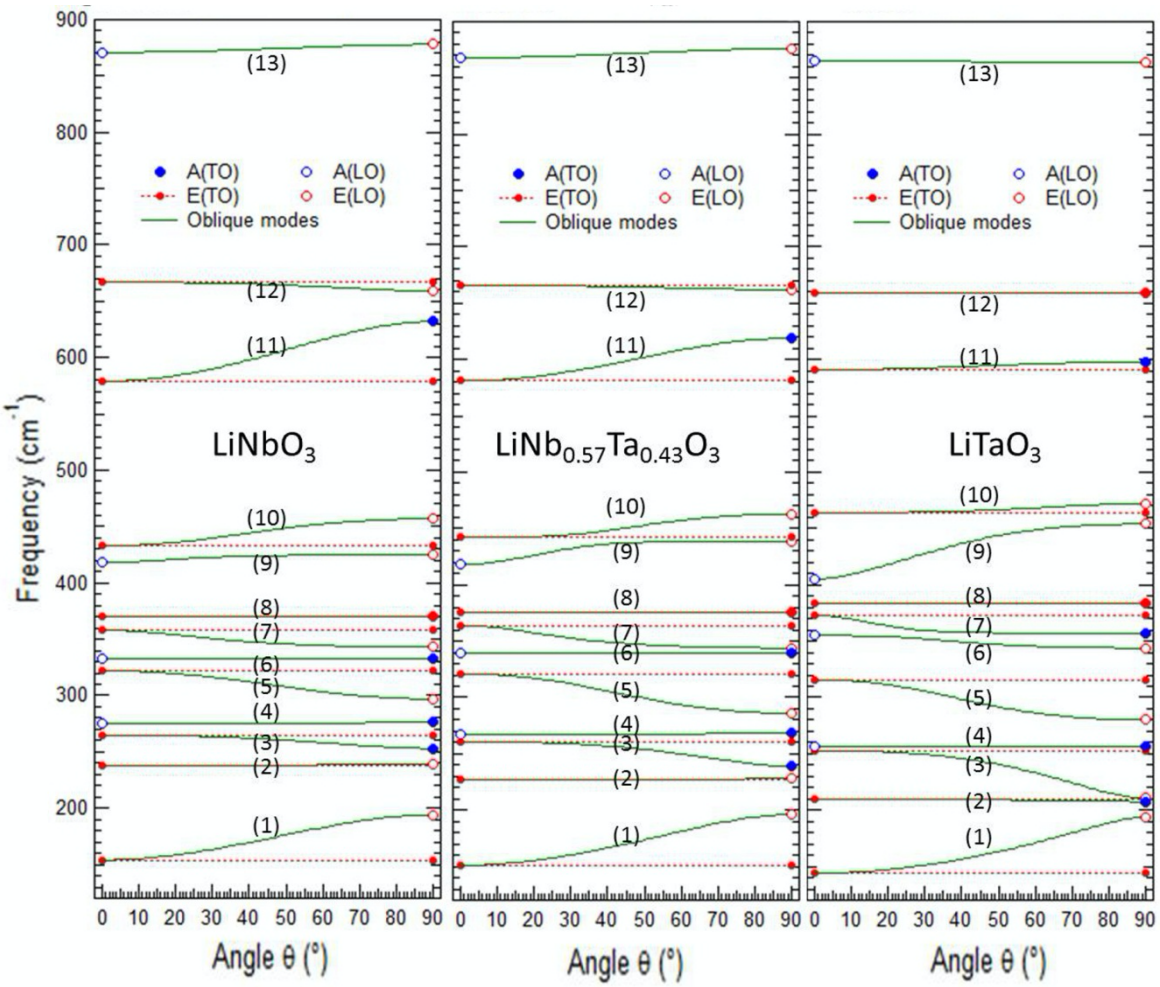

Fig. 8 Directional dispersion branches of extraordinary phonons of LN, $LNT_{0.43}$ and LT. Θ is the angle between the c-axis and the phonon wave vector.

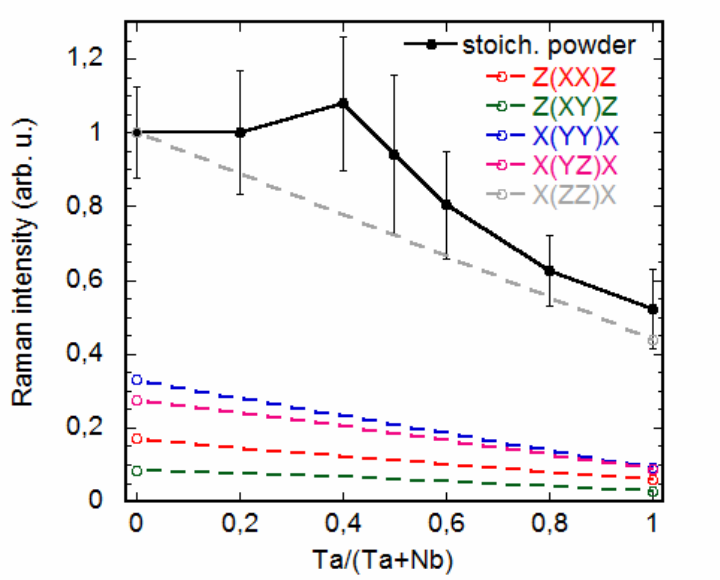

Fig. 9 The change of the total intensity of unpolarized Raman spectra with the Ta/Nb ratio in stoichiometric LNT_x powders. The integrated intensities of $Z(XX)\bar{Z}$, $Z(XY)\bar{Z}$, $X(YY)\bar{X}$, $X(YZ)\bar{X}$ and $X(ZZ)\bar{X}$ spectra of LN and L single crystals are given for comparison.

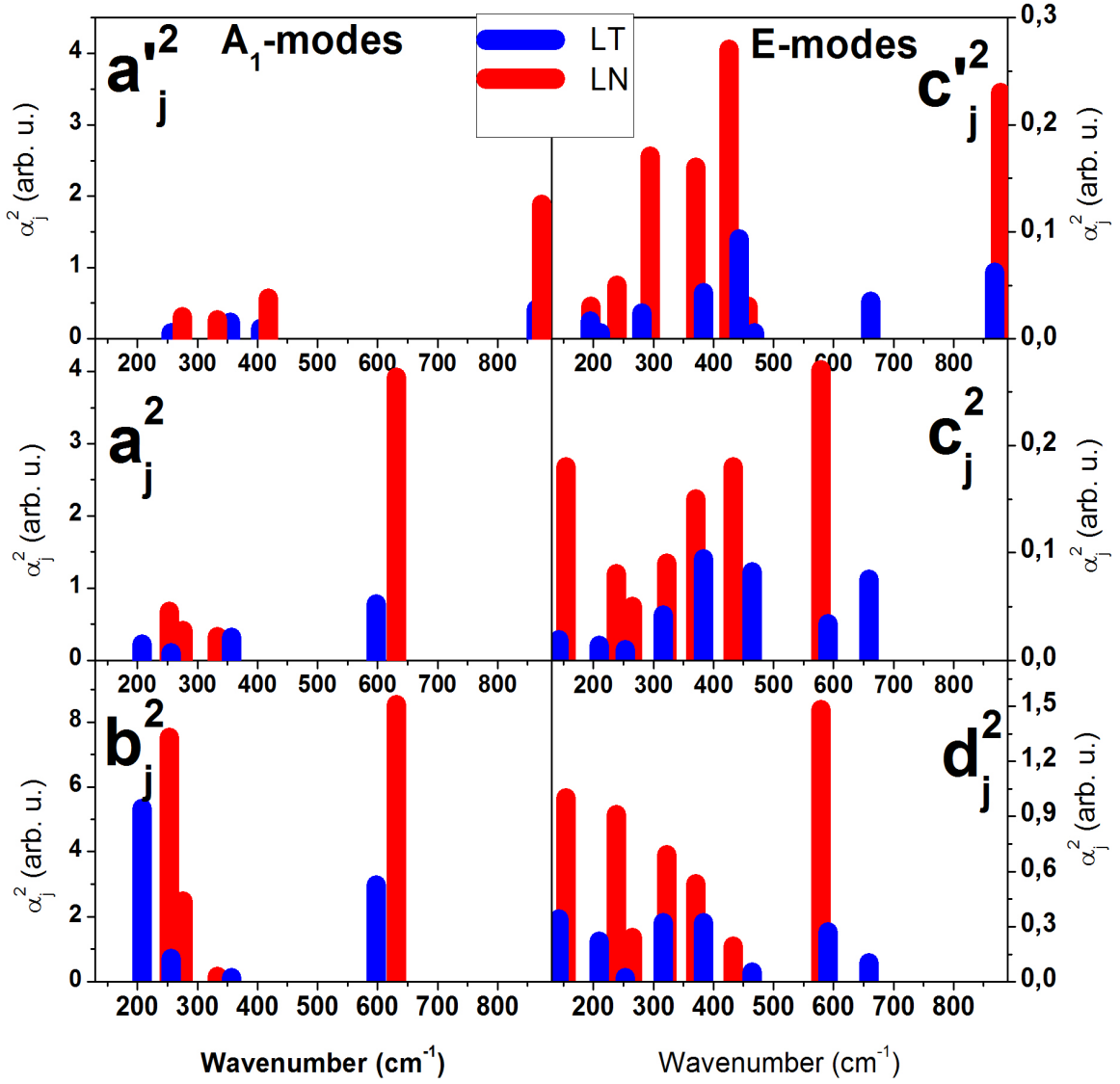

Fig. 10 Comparison of non-zero Raman tensor coefficients, α_j^2 , determining Raman efficiency of phonon modes of LN and LT crystals.

References

[1] S.C. Abrahams and J.L. Bernstein, Ferroelectric lithium tantalate—1. single crystal X-ray diffraction study at 24 C, J. Phys. Chem. Solid. 28, 1685 (1967).

[2] S.C. Abrahams, J.M. Reddy, and J.L. Bernstein, Ferroelectric lithium niobate. 3. Single crystal X-ray diffraction study at 24 C, J. Phys. Chem. Solid. 27, 997 (1966).

[3] A.M. Glazer, The classification of tilted octahedra in perovskites, Acta Cryst. B28, 3384 (1972).

[4] J.R. Carruthers, G.E. Peterson, M. Grasso, and P.M. Bridenbaugh, Nonstoichiometry and crystal growth of lithium niobate, J. Appl. Phys. 42, 1846 (1971).

[5] J.G. Bergman, A. Ashkin, A.A. Ballman, J.M. Dziedzic, H.J. Levinstein, and R.G. Smith, Curie temperature, birefringence, and phase-matching temperature variations in $LiNbO_3$ as a function of melt stoichiometry, Appl. Phys. Lett. 12, 92 (1967).

[6] A.A. Ballman, H.J. Levinstein, C.D. Capio, and H. Brown, Curie temperature and birefringence variation in ferroelectric lithium metatantalate as a function of melt stoichiometry, J. Am. Ceram. Soc. 50, 657 (1967).

[7] F. Shimura and Y. Fujino, Crystal growth and fundamental properties of $LiNb_{1-y}Ta_yO_3$, J. Cryst. Growth 38, 293 (1977).

[8] F. Shimura, Refractive indices of $LiNb_{1-y}Ta_yO_3$ single crystals, J. Cryst. Growth 42, 579 (1977).

[9] S. Margueron, A. Bartasyte, A.M. Glazer, E. Simon, J. Hlinka, I. Gregora, and J. Gleize, Resolved E-symmetry zone-centre phonons in $LiTaO_3$ and $LiNbO_3$, J. Appl. Phys. 111, 104105 (2012).

[10] A.F. Penna, A. Chaves, P. da R. Andrade, and S.P.S. Porto, Light scattering by lithium tantalate at room temperature, Phys. Rev. B 13, 4907 (1976).

[11] Jr. W.D. Johnston and I.P. Kaminow, Temperature dependence of Raman and Rayleigh scattering in $LiNbO_3$ and $LiTaO_3$, Phys. Rev. 168, 1045 (1968).

[12] Jr. A.S. Barker and R. Loudon, Dielectric properties and optical phonons in $LiNbO_3$, Phys. Rev. 158, 433 (1967).

[13] C. Raptis, Assignment and temperature dependence of the Raman modes of $LiTaO_3$ studied over the ferroelectric and paraelectric phases, Phys. Rev. B., 38, 10007 (1988).

[14] A.S. Barker, A.A. Ballman, and J.A. Ditzenberger, Infrared study of the lattice vibrations in $LiTaO_3$, Phys. Rev. B. 2, 4233 (1970).

[15] J.L. Servoin and F. Gervais, Analysis of infrared reflectivity in the presence of asymmetrical phonon lines, Appl. Optics 16, 2952 (1977).

[16] M.R. Chowdhury, G.E. Peckham, and D.H. Saunderson, A neutron inelastic scattering study of $LiNbO_3$, J. Phys. C: Solid State Phys. 11, 1671 (1978).

[17] P. Hermet, M. Veithen, and Ph. Ghosez, First-principles calculations of the nonlinear optical susceptibilities and Raman scattering spectra of lithium niobate, J. Phys.: Cond. Matter 19, 456202 (2007).

[18] V. Caciuc, A.V. Postnikov, and G. Borstel, Ab initio structure and zone-center phonons in $LiNbO_3$, Phys. Rev. B. 61, 8806 (2000).

[19] M. Veithen and Ph. Ghosez, First-principles study of the dielectric and dynamical properties of lithium niobate, Phys. Rev. B. 65, 214302 (2002).

[20] S. Sanna, S. Neufeld, M. Rusing, G. Berth, A. Zrenner, and W.G. Schmidt, Raman scattering efficiency in $LiNbO_3$ and $LiTaO_3$ crystals, Phys. Rev. B 91, 224302 (2015).

[21] R.J. Elliott and I.P. Ipatova, Optical properties of mixed crystals, Amsterdam : North-Holland Physics Publishing, ISBN: 0 444 87069 5 (1988).

[22] Y.-C. Ge and C.-Z. Zhao, Raman study of the phase transition in $LiTa_{0.9}Nb_{0.1}O_3$ single crystal, J. Raman Spectroscopy 26, 975 (1995).

[23] S. Sanna, A. Riefer, S. Neufeld, W.G. Schmidt, G. Berth, A. Widhalm, and A. Zrenner, Lithium niobate-tantalate mixed crystals electronic and optical properties calculated from first principles, IEEE ISAF proceedings (2012).

[24] M. Rusing, S. Sanna, S. Neufeld, G. Berth, W.G. Schmidt, A. Zrenner, H. Yu, Y. Wang, and H. Zhang, Vibrational properties of $LiNb_{1-x}Ta_xO_3$ mixed crystals, Phys. Rev. B 93, 184305 (2016).

[25] A. Bartasyte, V. Plausinaitiene, A. Abrutis, T. Murauskas, P. Boulet, S. Margueron, J. Gleize, S. Robert, V. Kubilius, and Z. Saltyte, Residual stresses and clamped thermal expansion in $LiNbO_3$ and $LiTaO_3$ thin films, Appl. Phys. Lett. 101, 122902 (2012).

[26] A.M. Glazer, N. Zhang, A. Bartasyte, D.S. Keeble, S. Huband, and P.A. Thomas, Observation of unusual temperature-dependent stripes in $LiTaO_3$ and $LiTa_xNb_{1-x}O_3$ crystals with near-zero birefringence, J. Appl. Cryst. 43 (6), 1305 (2010).

[27] A. Bartasyte, V.Plausinaitiene, A. Abrutis, S. Stanionyte, S. Margueron, P. Boulet, T. Kobata, Y. Uesu, and J. Gleize, Identification of $LiNbO_3$, $LiNb_3O_8$ and Li_3NbO_4 phases in thin films synthesized with different deposition techniques by means of XRD and Raman spectroscopy, J. Phys.: Condens. Matter 25, 205901 (2013).

[28] A. Bartasyte, S. Margueron, T. Baron, S. Oliveri, and P. Boulet, Toward high-quality epitaxial $LiNbO_3$ and $LiTaO_3$ thin films for acoustic and optical applications, Adv. Mater. Interfaces 4 (8), 1600998 (2017).

[29] R.H. Lyddane, R.G. Sachs, and E. Teller, On the polar vibrations of alkali halides, Phys. Rev. 59, 673 (1941).

[30] L. Merten, Phänomenologische Beschreibung der langen optischen Gitterschwingungen in zweiatomigen polaren Kristallen des trigonalen, tetragonalen und hexagonalen Systems (auf elektrostatischer Grundlage), Z. Naturforsch, 15a, 47 (1960).

[31] I.P. Kaminow and W.D. Johnston, Quantitative Determination of Sources of the Electro-Optic Effect in $LiNbO_3$ and $LiTaO_3$, Phys. Rev. 160, 519 (1967).

[32] A. Bartasyte, A.M. Glazer, F. Wondre, D. Prabhakaran, P.A. Thomas, S. Huband, D.S. Keeble, and S. Margueron, Growth of $LiNb_{1-x}Ta_xO_3$ solid solution crystals, Mater. Chem. Phys. 134, 728 (2012).

[33] S.M. Shapiro and J.D. Axe, Raman scattering from polar phonons, Phys. Rev. B 6, 2420 (1972).

[34] F. Gervais, Effective charges in binary and ternary oxide compounds, Solid State Com. 18, 191 (1976).

[35] I.P. Kaminow, An introduction to electrooptic devices, Academic Press, New York and London, ISBN: 0-12-395050-3 (1974).

[36] M. Schall, H. Helm, and S.R. Keiding, Far infrared properties of electro-optic crystals measured by THz time-domain spectroscopy, Int. J. Infrared and Milimeters Waves 20 (4), 595 (1999).

[37] G. Fini, P. Mirone, and P. Patella, Solvent effects on Raman band intensities, J. Mol. Spectrosc. 28, 144 (1968).

[38] I. Inbar and R.E. Cohen, Comparison of the electronic structures and energetics of ferroelectric $LiNbO_3$ and $LiTaO_3$, Phys. Rev. B 53 (3), 1193 (1996).